


Article

A Variational Bayesian and Huber-Based Robust Square Root Cubature Kalman Filter for Lithium-Ion Battery State of Charge Estimation

Jing Hou ^{1,†} , He He ², Yan Yang ^{1,*}, Tian Gao ¹ and Yifan Zhang ¹

¹ School of Electronic and Information, Northwestern Polytechnical University, Xi'an 710072, China; jhou0825@nwpu.edu.cn (J.H.); tiangao@nwpu.edu.cn (T.G.); shu@mail.nwpu.edu.cn (Y.Z.)

² System Engineering Research Institute of CSSC, Beijing 100094, China; hehe5951@163.com

* Correspondence: yangyan7003@nwpu.edu.cn

† Current address: No.127, Youyi West Road, Xi'an 710072, China.

Received: 2 March 2019; Accepted: 30 April 2019; Published: 7 May 2019



Abstract: An accurate state of charge (SOC) estimation is vital for safe operation and efficient management of lithium-ion batteries. To improve the accuracy and robustness, an adaptive and robust square root cubature Kalman filter based on variational Bayesian approximation and Huber's M-estimation (VB-HASRCKF) is proposed. The variational Bayesian (VB) approximation is used to improve the adaptivity by simultaneously estimating the measurement noise covariance and the SOC, while Huber's M-estimation is employed to enhance the robustness with respect to the outliers in current and voltage measurements caused by adverse operating conditions. A constant-current discharge test and an urban dynamometer driving schedule (UDDS) test are performed to verify the effectiveness and superiority of the proposed algorithm by comparison with the square root cubature Kalman filter (SRCKF), the VB-based SRCKF, and the Huber-based SRCKF. The experimental results show that the proposed VB-HASRCKF algorithm outperforms the other three filters in terms of SOC estimation accuracy and robustness, with a little higher computation complexity.

Keywords: state of charge (SOC); lithium-ion battery; square root cubature Kalman filter (SRCKF); variational Bayesian approximation; Huber's M-estimation; adaptive; robust

1. Introduction

Lithium-ion batteries have been prevalently employed as energy storage devices in electric vehicles (EVs) and renewable energy storage systems owing to their high energy density, low self-discharge rate, and long cycle life [1]. The state of charge (SOC), which represents the amount of charge remaining in a battery, is one of the most important indicators of the current performance of the battery. Therefore, the SOC needs to be accurately estimated by a battery management system (BMS) in order to achieve battery equalization, charging/discharging control, and driving distance forecast for electric vehicles. In addition, for the battery energy storage system (BESS) of the grid, accurate estimation of SOC is crucial for controlling the SOC level within a certain range in order to reserve a certain amount of energy for load leveling as well as minimize battery health degradation. Hence, the battery charging process is only allowed during off-peak hours if the SOC level of the battery is below a specified maximum value. Meanwhile, the discharge is activated during the peak hours for load leveling and prevented if the SOC is lower than a specified minimum value.

Nevertheless, it is difficult to directly measure the SOC since the battery itself is a highly nonlinear and time-varying system on account of its complicated internal electrochemical reaction. Moreover, SOC estimation accuracy is affected by various factors such as ambient temperature, battery aging,

and charging/discharging current rate[2]. Therefore, robust and accurate estimation of battery SOC is a difficult problem yet to be adequately resolved.

A great number of approaches have been proposed to estimate the SOC of lithium-ion batteries. The open-circuit voltage (OCV) method is a very simple one. But it needs a long rest time to measure the terminal voltage, making it almost impossible for moving vehicles. The coulomb counting (CC) method is widely applied in commercial BMSs, but its estimation accuracy depends heavily on the choice of the initial SOC values and suffers from measurement errors and accumulated errors. Machine learning algorithms including artificial neural networks (ANNs) [3–5], fuzzy logic (FL) algorithms [6–8], and support vector machines (SVMs) [9–11] have also been used for SOC estimation. These methods can estimate the SOC accurately and have no need for detailed physical knowledge of the battery. However, they require a large amount of experimental data to train the intelligent model beforehand. Moreover, the algorithms are easily divergent if the training data cannot completely cover the actual operating conditions [12].

Recently, model-based methods including observers [13,14], Kalman filter (KF), and its derivatives have been widely applied to SOC estimation. As the most representative method, the extended Kalman filter (EKF) was firstly introduced to estimate the SOC of a lithium-ion polymer battery by Plett [15] in 2004. But, EKF utilizes the first-order or second-order terms of Taylor's formula for linearization, which may bring in large linearization errors and thus degrade the SOC estimation accuracy. To overcome these defects, the unscented Kalman filter (UKF) [16–18] was put forward, which has a higher order of accuracy in estimating the mean and the error covariance of a state than EKF and does not need to calculate the Jacobian matrix. Ref. [19] evaluated the SOC estimation performance of the EKF, UKF, and particle filter (PF) for lithium-bismuth liquid metal batteries and showed that the UKF gave the most robust and accurate performance. Later, the cubature Kalman filter (CKF) [20,21] was proposed to improve the convergence rate and SOC estimation accuracy. CKF is based on the radial-spherical cubature rule, and is more suitable for state estimation of high-order nonlinear systems. Moreover, the cubature points and weights are uniquely determined by the dimension of the state, thus there is no need to tune parameters, as opposed to the UKF. Hence, it is easier for implementation. But asymmetric or non-positive definite covariance often arises during the iteration of CKF, which results in accuracy degradation or iteration interruption. To cope with the numerical instability of the CKF, square root cubature Kalman filter (SRCKF) [22,23] was developed, which can ensure the positive definiteness of the covariance. However, these KF-based methods also have some accuracy limitations. First, they are very sensitive to model mismatch, which can easily lead to filter divergence. Second, the process and measurement noise statistics are assumed to be known and Gaussian, which is not necessarily true in practical applications.

As we know that battery parameters change with SOC, temperature, and battery aging during the charge and discharge process, it is not easy to establish an exactly matched battery model. In other words, modeling error is usually inevitable. In addition, in complex industrial applications, the precision of current and voltage sensors is much lower than in the laboratory. Moreover, sensor noise is probably a non-Gaussian process with unknown or time-varying covariance. Therefore, to account for modeling error and contaminated distributions or outliers in measurements, an adaptive and robust SOC estimation method is badly required. To address the adaptivity, an adaptive square root unscented Kalman filter (ASRUKF) [24] and an adaptive cubature Kalman filter (ACKF) [21] based on the improved Sage–Husa estimator were presented. These methods adaptively adjusted the values of the process and measurement covariances in the estimation process to improve the accuracy of SOC estimation. El Din et al. [25] proposed a multiple-model EKF (MM-EKF) and an autocovariance least squares (ALS) method for estimating the SOC under measurement noise statistic uncertainties. MM-EKF reduced the impact caused by unknown measurement noise statistics by calculating the weighted sum of the estimates of multiple hypothesized EKFs. The ALS method extracted the possible correlation in the innovation sequence to estimate the measurement noise covariance. On the other hand, in order to improve the robustness of SOC estimation, H infinity filters [1,26–28] were employed

to deal with gross errors or outliers in measurements. However, when there are both modeling errors and outliers in the battery system, those filters cannot achieve satisfactory accuracy.

Actually, the variational Bayesian (VB)-based filter [29–33] is one of the most general adaptive filters. Its adaptive strategy has a strong ability to track the time-varying measurement noise covariance. Meanwhile, Huber's M-estimator [34] is a combined minimum l_1 and l_2 norm estimation technique, which exhibits robustness with respect to the contaminated distributions and outliers by modifying the filtering update. Thus, it will be promising to combine VB approximation and Huber's M-estimation to achieve both adaptivity and robustness. Li et al. [30] has acted out this idea in the framework of UKF. The efficiency of the proposed filter was verified through the numerical simulation test. In this paper, we extend this idea within the framework of SRCKF for adaptive and robust SOC estimation of the lithium-ion batteries. The measurement noise covariance is simultaneously estimated with the SOC to account for battery model uncertainties and measurement noise covariance uncertainties. Meanwhile, the outliers in current and voltage measurements caused by adverse operating conditions are accounted for by Huber's M-estimation. The effectiveness of the proposed filter has been verified through experiments under different operating conditions. The results show that the proposed filter can achieve much better estimation accuracy than SRCKF, the VB-based SRCKF, and the Huber-based SRCKF with a little higher computation complexity when there are both measurement outliers and mistuned measurement noise covariance.

The contributions of this paper are the following: (1) An adaptive and robust square root cubature Kalman filter based on variational Bayesian approximation and Huber's M-estimation (VB-HASRCKF) is proposed for SOC estimation of lithium-ion batteries; (2) Compared with the existing models, the case that there are both modeling errors and outliers in SOC estimation is firstly taken into account and the VB-HASRCKF is used to handle this problem; (3) A constant-current discharge test and an UDDS test are performed to verify the effectiveness and superiority of the proposed algorithm by comparison with the square root cubature Kalman filter (SRCKF), the VB-based SRCKF, and the Huber-based SRCKF.

The organization of this paper proceeds as follows: Section 2 describes the battery model and the parameter identification. Section 3 illustrates the VB-based adaptive SRCKF algorithm. In Section 4, the adaptive and robust SRCKF based on VB approximation and Huber's M-estimation is presented. The experimental verification and analysis are presented in Section 5. Finally, Section 6 provides a conclusion.

2. Battery Modeling and Parameter Identification

2.1. Battery Modeling

For the accurate estimation of the SOC, a reliable battery model is required. The existing models include the electrochemical model [35] and the equivalent circuit model (ECM) [24,28]. Among others, the ECMs have a better trade-off between accuracy and complexity. Therefore, we adopted a typical ECM, the first order resistor–capacitor (RC) model as shown in Figure 1, to model the lithium-ion battery in this paper.

The electrical behavior of the model can be written as follows:

$$\begin{aligned} U_t &= U_{oc} - U_1 - I_L R_0, \\ \dot{U}_1 &= \frac{I_L}{C_1} - \frac{U_1}{R_1 C_1}, \end{aligned}$$

where, U_t denotes the terminal voltage of the battery, U_{oc} is the open-circuit voltage, U_1 is the polarization voltage of the RC network, I_L is the load current, R_0 represents the ohmic internal resistance, and R_1 and C_1 represent the polarization resistance and polarization capacitance, respectively.

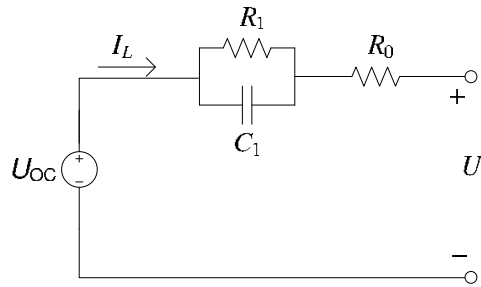


Figure 1. A first-order resistor–capacitor (RC) battery model.

The state of charge (SOC) is defined as the ratio of the remaining capacity in a battery over the maximum available capacity. Using the CC method, the battery SOC can be calculated as

$$SOC_t = SOC_{t_0} - \frac{1}{Q_{max}} \int_{t_0}^t \eta_c I_{L,t} dt,$$

where $I_{L,t}$ is the load current at time t , Q_{max} is the maximum available capacity of the battery, and η_c is the coulomb efficiency (CE), which is defined as the ratio of the discharge capacity to the charge capacity of the battery in the same cycle.

Here, we offer some explanations about CE. Theoretically, when a cell is free of undesired side reactions, its CE should permanently be 1.00 [36]. In fact, the CE value is not always equal to 1, and it is related to many battery parameters such as SOC, current rate, operating temperature, and battery capacity degradation. Zheng et al. [37] showed the correlation between SOC and CE and claimed that CE is almost invariant with SOC changes. The correlations of CE with current rate and operating temperature were discussed in [38,39]. Yang et al. [36] gave in-depth discussions regarding battery degradation, aging mechanisms, and CE evolution, and observed that a decrease of the CE value corresponds to an increase in the degradation rate and that an increase of the CE value indicates a decrease in the degradation rate. Meanwhile, experimental results also suggest that CE evolution is distinct for different types of batteries. Here, we do not consider the impact of these factors on CE and assume $\eta_c = 1$ since the CE of the lithium-ion battery is usually very high and has a fairly small measurement error. Moreover, this paper mainly focuses on handling the model uncertainties, which might also include the uncertainty brought by an inaccurate CE.

Taking $x = [SOC, U_1]^T$ as the state vector, the load current I_L as the input, and the terminal voltage U_t as the output, we can obtain the discrete state-space model as

$$\begin{aligned} x_{k+1} &= f(x_k, I_{L,k}) + w_k, \\ z_k &= U_{t,k} = h(x_k, I_{L,k}) + v_k, \end{aligned}$$

where $w_k \sim \mathcal{N}(0, Q_k)$ is the Gaussian process noise with covariance Q_k , and $v_k \sim \mathcal{N}(0, R_k)$ is the measurement noise with variance R_k . $f(\cdot)$ and $h(\cdot)$ represent the nonlinear functions of state vector x_k and input $I_{L,k}$. Their mathematical expressions are

$$\begin{aligned} f(\cdot) &= \begin{bmatrix} 1 & 0 \\ 0 & e^{-\frac{\Delta t}{\tau_1}} \end{bmatrix} \begin{bmatrix} SOC_k \\ U_{1,k} \end{bmatrix} + \begin{bmatrix} -\frac{\eta \Delta t}{Q_{max}} & 0 \\ 0 & R_1(1 - e^{-\frac{\Delta t}{\tau_1}}) \end{bmatrix} I_{L,k}, \\ h(\cdot) &= U_{OC}(SOC_k) - U_{1,k} - I_{L,k} R_0, \end{aligned}$$

where Δt is the sampling interval of the current, and $\tau_1 = R_1 C_1$ is the time constant of the RC network. $U_{OC}(SOC_k)$ represents the nonlinear relationship between the open-circuit voltage and the SOC, which is determined by experiments in the next section.

2.2. OCV–SOC Relationship Determination

In order to acquire the relationship between OCV and SOC, the following test procedure was designed:

- (1) First, fully charge the battery and rest for 1 h to finish the process of depolarization. Then the measured terminal voltage is assumed to be the discharge OCV value.
- (2) Discharge the battery at a constant current of 1A until 10% of the maximum available capacity is consumed, and measure the OCV after resting for 1 h.
- (3) Repeat step (2) until the battery reaches its lower cut-off voltage.

Based on the measured data, a fifth-order polynomial in Equation (1) is selected to characterize the relationship between OCV and SOC, and the measured data and fitted curve are presented in Figure 2. The R-squared is used to represent the goodness of fit. The normal value range of the R-squared is 0 – 1 and the closer to 1, the better for curve fitting [40]. It can be seen that the curve fits well with the measurement data, indicating that the selected fifth-order polynomial model can describe the relationship between OCV and SOC very well.

$$U_{oc}(SOC) = 3.083 + 4.859 \times SOC - 18.21 \times SOC^2 + 38.56 \times SOC^3 - 38.64 \times SOC^4 + 14.58 \times SOC^5. \quad (1)$$

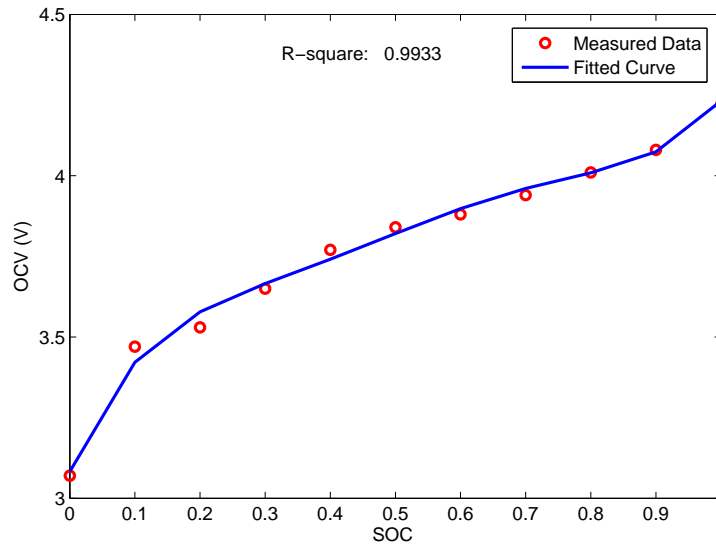


Figure 2. The relationship curve of open-circuit voltage (OCV) versus state of charge (SOC).

2.3. Online Parameter Identification

The battery model parameters are changeable with the operating current, SOC, temperature and aging, so that offline identification of model parameters will inevitably lead to some model errors. Therefore, in this paper the model parameters are updated online using the forgetting factor recursive least squares (FFRLS) algorithm [21] to improve the SOC estimation accuracy.

The transfer function of the battery model can be written as

$$G(s) = \frac{(U_{oc} - U_t)(s)}{I_L(s)} = \frac{R_1}{1 + R_1 C_1 s} + R_0. \quad (2)$$

Using $X(s) = \frac{X(k) - X(k-1)}{T}$ to discretize Equation (2), where T is the sampling period, we can obtain

$$\left(\frac{R_1 C_1}{T} + 1\right)(U_{oc} - U_t)(k) = \frac{R_1 C_1}{T}(U_{oc} - U_t)(k-1) + \left(\frac{R_0 R_1 C_1}{T} + R_0 + R_1\right)I_L(k) - \frac{R_0 R_1 C_1}{T}I_L(k-1). \quad (3)$$

Replacing the coefficients in Equation (3) with k_1 , k_2 , and k_3 , we can get

$$(U_{oc} - U_t)(k) = -k_1(U_{oc} - U_t)(k-1) + k_2 I_L(k) + k_3 I_L(k-1). \quad (4)$$

Define

$$\begin{cases} \varphi(k) = [-(U_{oc} - U_t)(k-1); I_L(k); I_L(k-1)] \\ \theta(k) = [k_1; k_2; k_3] \\ y(k) = (U_{oc} - U_t)(k). \end{cases}$$

The discrete time-domain difference expression in Equation (4) can be rewritten as

$$y(k) = \varphi^T(k)\theta(k) + \zeta(k), \quad (5)$$

where ζ is a Gaussian random noise with zero mean.

The vector $\theta(k)$ in Equation (5) can be solved using the FFRLS algorithm with forgetting factor λ (typically $\lambda = [0.95, 1]$), formulated as

$$\begin{cases} \hat{\theta}(k) = \hat{\theta}(k-1) + K(k)[y(k) - \varphi^T(k)\hat{\theta}(k-1)] \\ K(k) = \frac{P(k-1)\varphi(k)}{\lambda + \varphi^T(k)P(k-1)\varphi(k)} \\ P(k) = \frac{1}{\lambda}[I - K(k)\varphi^T(k)]P(k-1). \end{cases}$$

Finally, R_0 , R_1 , and C_1 can be derived by

$$\begin{cases} R_0 = \frac{k_3}{k_1} \\ R_1 = \frac{k_2 - R_0}{k_1 + 1} \\ C_1 = \frac{-k_1 T}{(k_1 + 1)R_1}. \end{cases}$$

2.4. Model Validation

The battery model described in this paper was verified through a 1A constant-current discharge test and UDDS test. The measured terminal voltage and the model terminal voltage were compared, as shown in Figures 3 and 4. The maximum absolute error was 0.045 V, while the mean absolute error was 0.0017 V in the constant-current discharge test. The maximum and mean absolute errors were 0.091 V and 0.0047 V in the UDDS test, respectively. It is clear that the model terminal voltage agrees well with the measured voltage. This illustrates the effectiveness of the battery model.

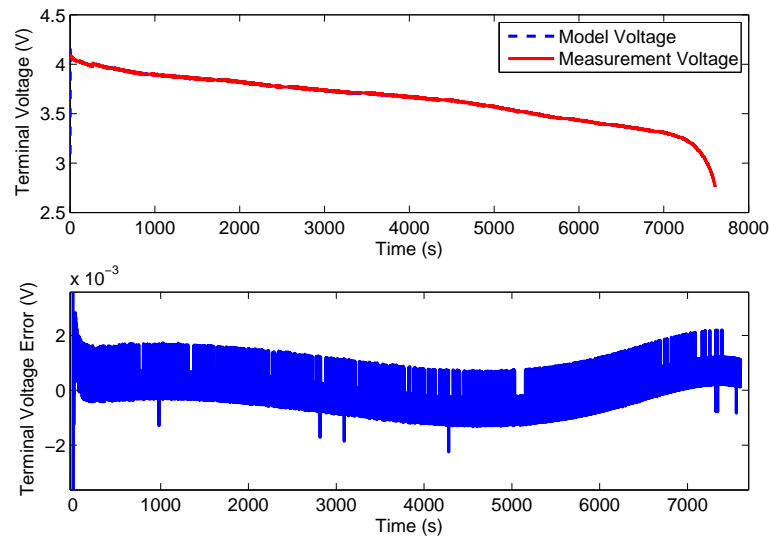


Figure 3. Experimental terminal voltage results in a constant-current discharge test.

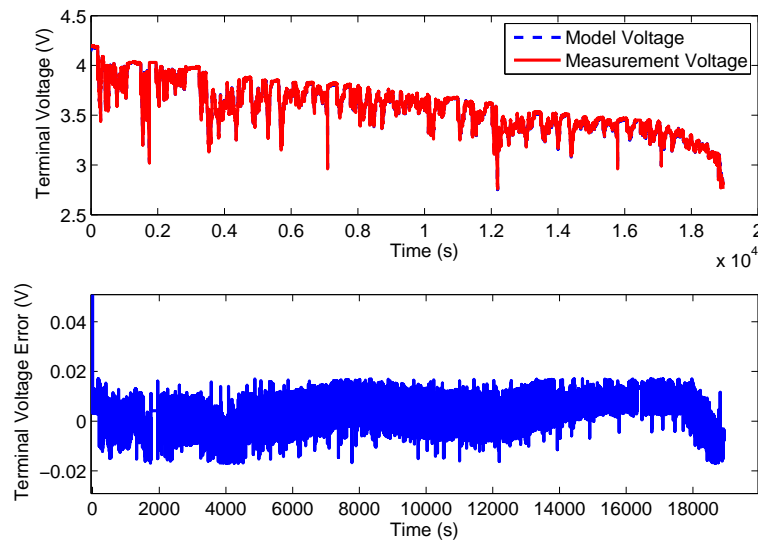


Figure 4. Experimental terminal voltage results in an urban dynamometer driving schedule (UDDS) test.

3. Variational Bayesian-Based Adaptive Square Root Cubature Kalman Filter

Recently, the variational Bayesian (VB)-based filter, which has a strong ability to track the uncertain parameters, has drawn extensive attention. In [29], a VB approximation-based adaptive Kalman filter was first presented, which can be used for the measurement of noise covariance adaptation. For nonlinear systems, a VB-based UKF is developed in [30]. Here, we focus on the adaptive square root cubature Kalman filter (SRCKF) based on VB approximation.

Let us rewrite the state-space equations for SOC estimation as

$$\begin{cases} x_{k+1} = f(x_k, I_{L,k}) + w_k \\ z_k = h(x_k, I_{L,k}) + v_k \\ w_k \sim \mathcal{N}(0, Q_k) \\ v_k \sim \mathcal{N}(0, R_k), \end{cases}$$

where the process noise covariance Q_k is assumed to be known, and the measurement noise covariance R_k is unknown.

The VB-based adaptive filter uses VB approximation to estimate the joint posterior distribution of the state and covariance $p(x_k, R_k | z_{1:k})$, as follows:

$$p(x_k, R_k | z_{1:k}) \approx Q_x(x_k) Q_R(R_k).$$

The VB approximation can now be formed by minimizing the Kullback–Leibler (KL) divergence between the separable approximation and the true posterior:

$$\begin{aligned} & KL[Q_x(x_k) Q_R(R_k) || p(x_k, R_k | z_{1:k})] \\ &= \int Q_x(x_k) Q_R(R_k) \times \log \left(\frac{Q_x(x_k) Q_R(R_k)}{p(x_k, R_k | z_{1:k})} \right) dx_k dR_k. \end{aligned}$$

Minimizing the KL divergence with respect to the probability densities $Q_x(x_k)$ and $Q_R(R_k)$ in turn, while keeping the other fixed, we can get the following equations:

$$Q_x(x_k) \propto \exp \left(\int \log p(z_k, x_k, R_k | z_{1:k-1}) Q_R(R_k) dR_k \right),$$

$$Q_R(R_k) \propto \exp \left(\int \log p(z_k, x_k, R_k | z_{1:k-1}) Q_x(x_k) dx_k \right).$$

Computing the above equations, we can get the following densities [29]:

$$Q_x(x_k) = \mathcal{N}(x_k | \hat{x}_k, P_k),$$

$$Q_R(R_k) = \text{IW}(R_k | v_k, V_k),$$

where $\text{IW}(\cdot)$ represents the inverse Wishart (IW) distribution, and the parameters \hat{x}_k , P_k , v_k , and V_k can be calculated using Kalman-type filters.

The above are the basic idea of the adaptive Kalman filter based on VB approximation. To solve the nonlinear battery SOC estimation problem, the VB method is rewritten in the SRCKF framework in this paper. The filtering procedure of the VB-based adaptive SRCKF algorithm (VB-ASRCKF) is summarized as follows.

Step 1. Initialize state and parameter estimation: \hat{x}_0 , S_0 , Q_0 , v_0 , V_0 .

Step 2. Predict ($k = 1, 2, 3, \dots$).

Step 2.1 Calculate the cubature points

$$X_{i,k-1} = S_{k-1} \xi_i + \hat{x}_{k-1} \quad i = 1, 2, \dots, 2n, \quad (6)$$

where ξ_i is the i th column of the weight matrix of the cubature points $[nI_n \quad -nI_n]$, I_n is the $n \times n$ identity matrix, and n is the dimension of the state vector.

Step 2.2 Propagate the cubature points through the process equation and calculate the predicted state values:

$$\chi_{i,k|k-1} = f(X_{i,k-1}, I_{L,k-1}), \quad (7)$$

$$\hat{x}_{k|k-1} = \frac{1}{2n} \sum_{i=1}^{2n} \chi_{i,k|k-1}. \quad (8)$$

Step 2.3 Calculate the square root of the covariance of the predicted state

$$S_{k|k-1} = \text{Tri}a([\chi_{k|k-1}^* \quad S_{Q,k-1}]^T), \quad (9)$$

where $S = \text{Tri}a(A)$ represents the QR decomposition of matrix A , which obtains a unitary matrix B and an upper triangular matrix C . We define $S = C^T$. $S_{Q,k-1}$ is the Cholesky decomposition of Q_{k-1} . That is, $Q_{k-1} = S_{Q,k-1} S_{Q,k-1}^T$. In addition,

$$\chi_{k|k-1}^* = \frac{1}{\sqrt{2n}} [\chi_{1,k|k-1} - \hat{x}_{k|k-1}, \dots, \chi_{2n,k|k-1} - \hat{x}_{k|k-1}]. \quad (10)$$

Step 2.4 Calculate the parameters of the IW distribution of measurement noise covariance

$$v_{k|k-1} = \rho(v_{k-1} - n - 1) + n + 1, \quad (11)$$

$$V_{k|k-1} = B V_{k-1} B^T, \quad (12)$$

where ρ is a scale factor that $0 < \rho \leq 1$ and B is a matrix that $0 < |B| \leq 1$ with a reasonable choice for the matrix $B = \sqrt{\rho} I_d$. I_d is an identity matrix and d is the dimension of the measurement.

Step 3. Update: the update of VB-ASRCKF utilizes an iterate filtering framework.

Step 3.1 First set $\hat{x}_k^{(0)} = \hat{x}_{k|k-1}$, $S_k^{(0)} = S_{k|k-1}$, $V_k^{(0)} = V_{k|k-1}$, and $v_k = 1 + v_{k|k-1}$.

Step 3.2 Calculate the cubature points of the predicted state

$$X_{i,k|k-1} = S_{k|k-1} \xi_i + \hat{x}_{k|k-1}. \quad (13)$$

Step 3.3 Propagate the cubature points through the measurement equation and calculate the predicted measurement value

$$Z_{i,k|k-1} = h(X_{i,k|k-1}), \quad (14)$$

$$\hat{z}_{k|k-1} = \frac{1}{2n} \sum_{i=1}^{2n} Z_{i,k|k-1}. \quad (15)$$

Step 3.4 Calculate the covariance of the state and the measurement

$$P_{xz,k|k-1} = \chi_{k|k-1} Z_{k|k-1}^T, \quad (16)$$

where

$$\chi_{k|k-1} = \frac{1}{\sqrt{2n}} [X_{1,k|k-1} - \hat{x}_{k|k-1}, \dots, X_{2n,k|k-1} - \hat{x}_{k|k-1}], \quad (17)$$

$$Z_{k|k-1} = \frac{1}{\sqrt{2n}} [Z_{1,k|k-1} - \hat{z}_{k|k-1}, \dots, Z_{2n,k|k-1} - \hat{z}_{k|k-1}]. \quad (18)$$

Step 3.5 For $j = 1 : N$, iterate the following N (N denotes iterated times) steps.

Step 3.5.1 Calculate the measurement covariance

$$R_k^{(j)} = (v_k - n - 1)^{-1} V_k^{(j-1)}. \quad (19)$$

Step 3.5.2 Calculate the square root of the innovation covariance

$$S_{zz,k|k-1}^{(j)} = \text{Tria}([Z_{k|k-1} \ S_{R,k}^{(j)}]^T), \quad (20)$$

Step 3.5.3 where $S_{R,k}^{(j)}$ is the Cholesky decomposition of $R_k^{(j)}$. Calculate the filter gain

$$K_k^{(j)} = \frac{P_{xz,k|k-1} [S_{zz,k|k-1}^{(j)}]^{-1}}{S_{zz,k|k-1}^{(j)}}. \quad (21)$$

Step 3.5.4 Calculate the state estimate and the square root of its covariance

$$\hat{x}_k^{(j)} = \hat{x}_{k|k-1} + K_k^{(j)} (z_k - \hat{z}_{k|k-1}), \quad (22)$$

$$S_k^{(j)} = \text{Tria}([\chi_{k|k-1} - K_k^{(j)} Z_{k|k-1} \ K_k^{(j)} S_{R,k}^{(j)}]^T). \quad (23)$$

Step 3.5.5 Calculate the updated parameter of the IW distribution of measurement noise covariance

$$X_{i,k}^{(j)} = S_k^{(j)} \xi_i + \hat{x}_k^{(j)}, \quad (24)$$

$$V_k^{(j)} = V_{k|k-1} + \frac{1}{2n} \sum_{i=1}^{2n} (z_k - h(X_{i,k}^{(j)}))(z_k - h(X_{i,k}^{(j)}))^T. \quad (25)$$

Step 3.6 Until $j = N$, set $\hat{x}_k = \hat{x}_k^{(N)}$, $S_k = S_k^{(N)}$, $V_k = V_k^{(N)}$, and end for. Then one cycle of the VB-ASRCKF algorithm is finished.

4. Variational Bayesian and Huber-Based Robust Square Root Cubature Kalman Filter

In adverse environments, the current and voltage sensor noises maybe non-Gaussian, or there may be outliers in the voltage and current measurements. In this case, the above adaptive filter is incapable of achieving good performance. As we know, Huber's M-estimation method is a combined minimum l_1 and l_2 norm estimation technology, which exhibits robustness with respect to non-Gaussian distributions and outliers [34]. Therefore, to account for the measurement noise covariance uncertainties as well as the non-Gaussian distributions or outliers in the measurements for the battery SOC estimation, VB approximation and Huber's M-estimation-based square root cubature Kalman filter (VB-HASRCKF) with adaptivity and robustness is proposed.

First, let's give an introduction to Huber's M-estimation. The update of the filter can be viewed as a solution to a particular weighted least squares problem; we can construct the nonlinear regression measurement model as

$$\begin{bmatrix} z_k \\ \hat{x}_{k|k-1} \end{bmatrix} = \begin{bmatrix} h(x_k) \\ x_k \end{bmatrix} + \begin{bmatrix} v_k \\ \delta \hat{x}_{k|k-1} \end{bmatrix}, \quad (26)$$

where $\hat{x}_{k|k-1}$ is the prediction of the state with covariance $P_{k|k-1}$, and $\delta \hat{x}_{k|k-1}$ is the error between the true state and its prediction. Through the definition of the quantities

$$W_k = \begin{bmatrix} R_k & 0 \\ 0 & P_{k|k-1} \end{bmatrix}, \quad (27)$$

$$y_k = W_k^{-1/2} \begin{bmatrix} z_k \\ \hat{x}_{k|k-1} \end{bmatrix}, \quad (28)$$

$$g(x_k) = W_k^{-1/2} \begin{bmatrix} h(x_k) \\ x_k \end{bmatrix}, \quad (29)$$

$$\varepsilon_k = W_k^{-1/2} \begin{bmatrix} v_k \\ \delta \hat{x}_{k|k-1} \end{bmatrix}, \quad (30)$$

the above Equation (26) is integrated into

$$y_k = g(x_k) + \varepsilon_k. \quad (31)$$

Define Huber's generalized cost function as

$$J(x_k) = \sum_{i=1}^{n+d} \rho(e_{i,k}), \quad (32)$$

where n and d are the dimensions of the state and the measurement, respectively. $e_k = y_k - g(x_k)$ is the residual error, $e_{i,k}$ is the i th component of e_k , and ρ is defined as

$$\rho(e_{i,k}) = \begin{cases} e_{i,k}^2/2 & |e_{i,k}| < \gamma \\ \gamma|e_{i,k}| - \gamma^2/2 & |e_{i,k}| \geq \gamma \end{cases}, \quad (33)$$

where γ is a tuning parameter to be chosen to give the desired efficiency to the Gaussian model.

Minimizing (32), we can find the implicit solution to the nonlinear regression problem as

$$\sum_{i=1}^{n+d} \phi(e_{i,k}) \frac{\partial e_{i,k}}{\partial x_i} = 0, \quad (34)$$

where $\phi(e_{i,k}) = \rho'(e_{i,k})$.

Define

$$\psi(e_{i,k}) = \phi(e_{i,k})/e_{i,k} = \begin{cases} 1 & |e_{i,k}| < \gamma \\ \text{sgn}(e_{i,k})\gamma/e_{i,k} & |e_{i,k}| \geq \gamma \end{cases}, \quad (35)$$

and let $\Psi = \text{diag}[\psi(e_{i,k})]$. Then, Ψ can be used to reformulate the measurement information. There are two ways to reformulate the measurement information.

One way is to re-weight the residual error covariance by assigning smaller weights to outlying observations. Denote \tilde{W}_k as the modified measurement noise covariance, that is

$$\tilde{W}_k = W_k^{1/2} \Psi^{-1} (W_k^{1/2})^T.$$

Then, denote \tilde{R}_k as the modified measurement covariance with $\tilde{R}_k = \tilde{W}_k(1:d, 1:d)$. Replacing R_k with \tilde{R}_k will lead to the robust filter.

Another way is to re-construct the “pseudo observations” by truncating the too-large or too-small observations. When $|e_{i,k}| \geq \gamma$, replace $e_{i,k}$ with $\text{sign}(e_{i,k})\gamma$. Denote \tilde{e}_k as the modified residual error and $\tilde{e}_k = \Psi e_k$, which is the same to modify the measurements y_k . Denote \tilde{y}_k as the modified y_k by

$$\tilde{y}_k = g(x_k) + \tilde{e}_k. \quad (36)$$

We can get the modified original measurement \tilde{z}_k as

$$\tilde{z}_k = W_k^{1/2} \tilde{y}_k(1:d) = W_k^{1/2} [g(x_k) + \Psi(1:d, 1:d) e_k(1:d)]. \quad (37)$$

Replacing z_k with \tilde{z}_k will also lead to the robust filter. Moreover, the two methods have the same robust performance. In this paper, we will select the second method to modify the measurements. The detailed reasons can be found in [30].

Considering the case under which there is both unknown measurement noise covariance and outliers in the measurements, Huber’s M-estimation is integrated with VB approximation within the SRCKF framework in this paper. The filtering procedure of the proposed VB-HASRCKF algorithm is summarized as follows.

Step 1. Initialize: $\hat{x}_0, S_0, Q_0, v_0, V_0$.

Step 2. Predict: using equations (6)–(12) to obtain $\hat{x}_{k|k-1}, S_{k|k-1}, V_{k|k-1}$, and $v_{k|k-1}$.

Step 3. Update.

Step 3.1 Using (13)–(18) to obtain $Z_{k|k-1}, \chi_{k|k-1}, \hat{z}_{k|k-1}$, and $P_{xz,k|k-1}$.

Step 3.2 Set $\hat{x}_k^{(0)} = \hat{x}_{k|k-1}, S_k^{(0)} = S_{k|k-1}, V_k^{(0)} = V_{k|k-1}$, and $v_k = 1 + v_{k|k-1}$.

Step 3.3 For $j = 1 : N$, iterate the following N (N denotes iterated times) steps.

Step 3.3.1 Use (19)–(21) to calculate $R_k^{(j)}, S_{zz,k|k-1}^{(j)}$ and $K_k^{(j)}$.

Step 3.3.2 Calculate \tilde{z}_k using (26)–(35) and (36)–(37).

Step 3.3.3 Replace z_k with \tilde{z}_k in (22)–(25). That is, proceed with the following calculations:

$$\begin{aligned}\hat{x}_k^{(j)} &= \hat{x}_{k|k-1} + K_k^{(j)}(\tilde{z}_k - \hat{z}_{k|k-1}), \\ S_k^{(j)} &= \text{Tri}a([\chi_{k|k-1} - K_k^{(j)}Z_{k|k-1} \quad K_k^{(j)}S_{R,k}^{(j)T}), \\ X_{i,k}^{(j)} &= S_k^{(j)}\xi_i + \hat{x}_k^{(j)}, \\ V_k^{(j)} &= V_{k|k-1} + \frac{1}{2n} \sum_{i=1}^{2n} (\tilde{z}_k - h(X_{i,k}^{(j)}))(\tilde{z}_k - h(X_{i,k}^{(j)}))^T,\end{aligned}$$

where $S_{R,k}^{(j)}$ is the Cholesky decomposition of $R_k^{(j)}$.

Step 3.4 Until $j = N$, set $\hat{x}_k = \hat{x}_k^{(N)}$, $S_k = S_k^{(N)}$, $V_k = V_k^{(N)}$ and end for. Then one cycle of the VB-HASRCKF algorithm is finished.

5. Experimental Verification and Analysis

5.1. Experimental Settings

To evaluate the effectiveness of the proposed method, a test bench shown in Figure 5 is established. The test bench consists of a lithium-ion battery cell, an electronic load, and a host computer. The tested lithium-ion battery cell is type ICR18650 developed by SAMSUNG, whose nominal capacity is 2.6 Ah, nominal voltage is 3.63 V, and charging and discharging cutoff voltages are 4.2 V and 2.75 V, respectively. The type of electronic load is IT8516S produced by ITECH, whose current measurement accuracy is $\pm(0.1\% + 0.1\% \text{ full scale})$ and voltage measurement accuracy is $\pm(0.02\% + 0.02\% \text{ full scale})$.

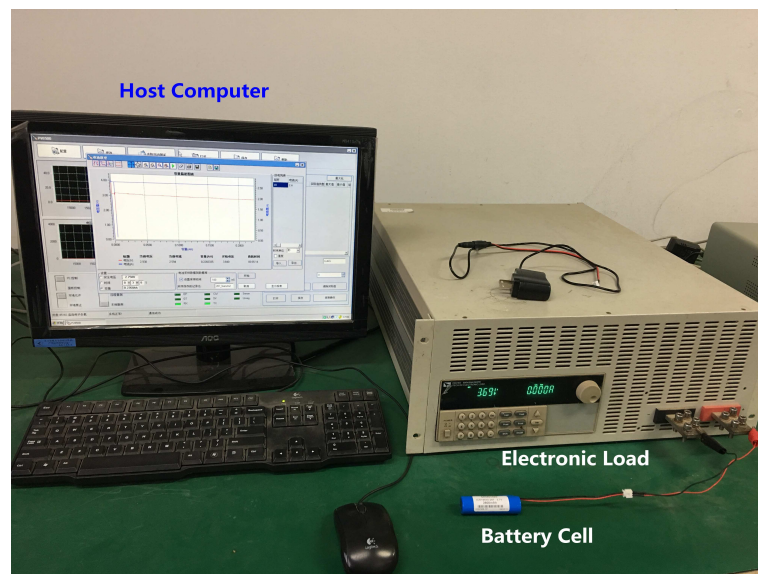


Figure 5. The experimental setup.

A constant-current discharge test and an urban dynamometer driving schedule (UDDS) test were performed to validate the proposed VB-HASRCKF algorithm on the basis of the test bench. The current, voltage, and SOC can be recorded via the host computer. The battery current and voltage were both sampled at 1 second. In each test, the true SOC was obtained using the CC method, and the estimation accuracy and robustness of the proposed VB-HASRCKF were evaluated by comparison with SRCKF, Huber-based SRCKF (HSRCKF), and VB-ASRCKF under different tests and different kinds of violations:

- Case a:** without any outliers or mistuning;
Case b: with mistuned measurement noise covariance;
Case c: with outliers in the measurements;
Case d: with both mistuned measurement noise covariance and outliers in the measurements.

5.2. SOC Estimation Experimental Results under a 1A Constant-Current Discharge Test

The experiment was performed with a constant discharge current of 1A. The initial SOC value was set to be 0.8, different from the real SOC of 1.0. The process noise covariance was set as $Q_k = 1 \times 10^{-8} I_2$. The measurement noise variance used for SRCKF and HSRCKF was assumed to be $R_k = 0.01$ in cases *a* and *c*, while mistuned to $R_k = 0.1$ in cases *b* and *d*. The initial parameter values of VB-based filters were $v_0 = 100$ and $V_0 = 1$ in cases *a* and *c*, and $v_0 = 100$ and $V_0 = 10$ in cases *b* and *d*. For cases *c* and *d*, some outliers in the voltage and current measurements were artificially added on the basis of the real experiment data. Figure 6 presents the contaminated current and voltage measurements. The outlying voltage measurements began at time $k = 100$ s, 1000 s, 2000 s, and 3000 s, and lasted for 3~10 s. The outliers in the current measurements were added at time $k = 100$ s and $k = 1000$ s.

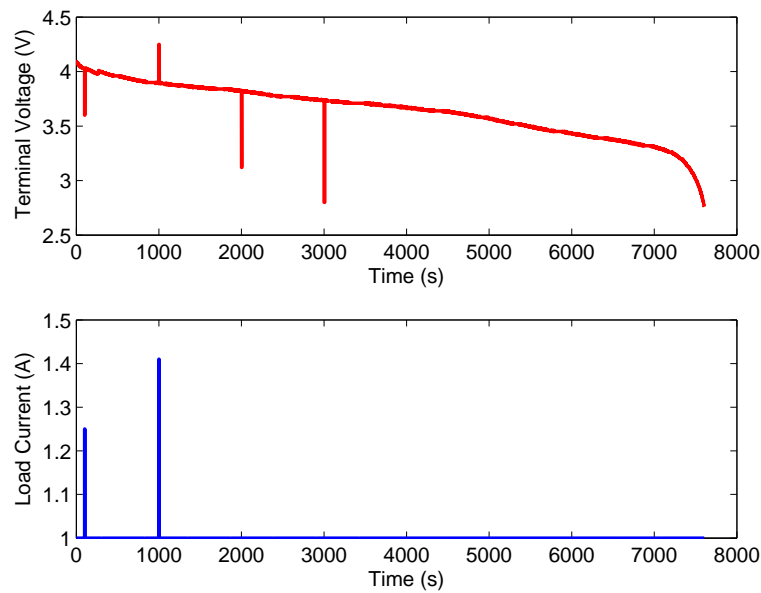


Figure 6. The outlying voltage and current measurements in a constant-current discharge test under cases *c* and *d*.

The SOC estimation results using SRCKF, HSRCKF, VB-ASRCKF, and VB-HASRCKF under four cases are shown in Figures 7 and 8. The maximum and mean absolute estimation errors are shown in Table 1. Meanwhile, the estimated measurement variances are presented in Figure 9. As can be seen in Figure 7a and Table 1, in case *a*, the mean absolute error of the four filters is around 0.70%, so they have comparable SOC estimation accuracy. Meanwhile, the converge rates of all the filters are also comparable since the SOC estimation errors are almost immediately decreased to under 5% for all filters. In addition, as shown in Figure 9, the estimated measurement noise variances of VB-ASRCKF and VB-HASRCKF are about 0.02, which does not deviate too much from the assumed variances of SRCKF and HSRCKF. It shows that the assumed measurement noise variance is consistent with the actual value. Therefore, the four filters display comparable performance.

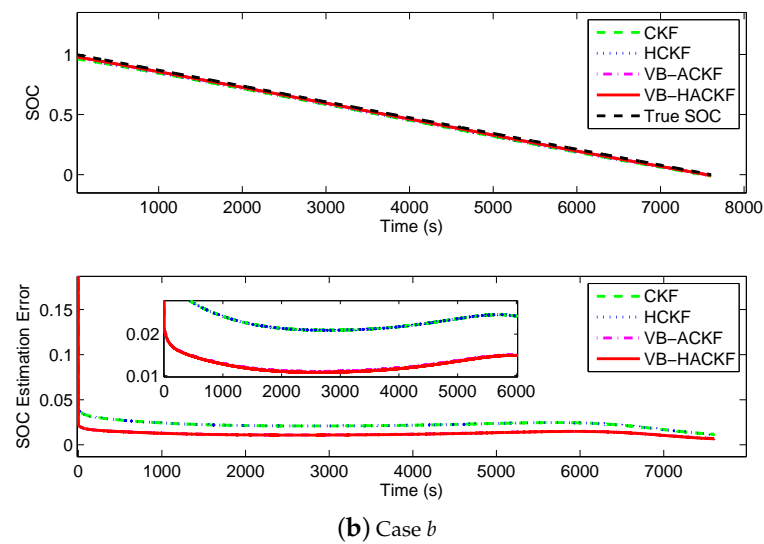
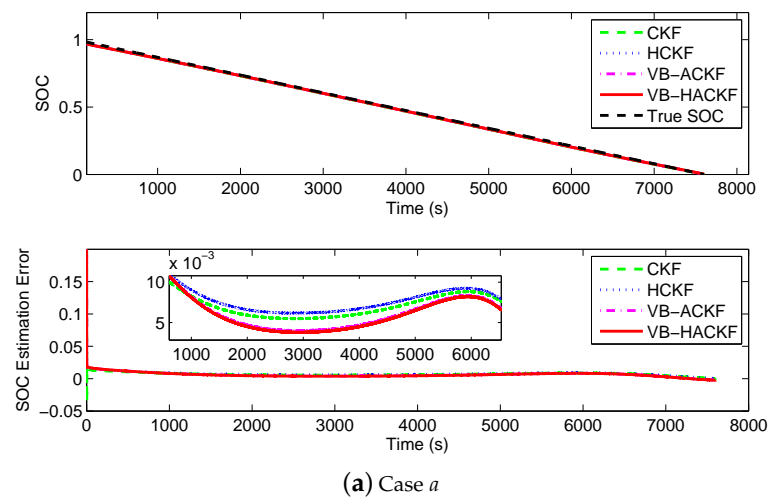


Figure 7. SOC estimation results of four filters in a constant-current discharge test under cases *a* and *b*.

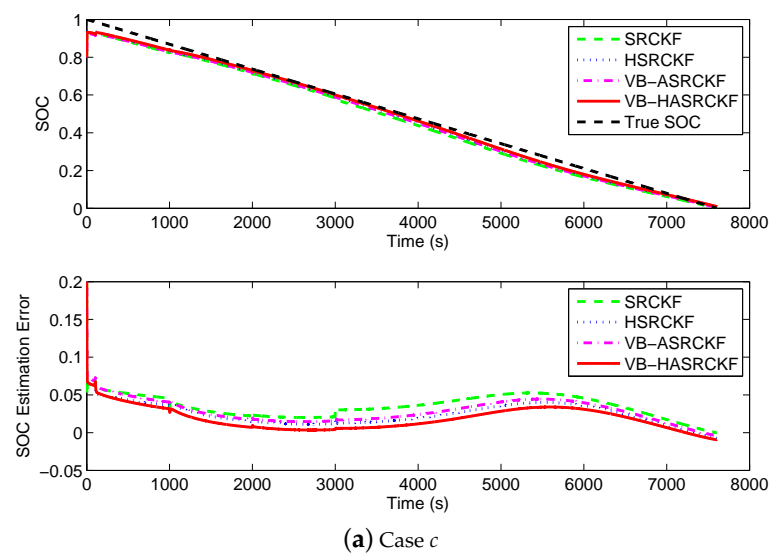


Figure 8. Cont.

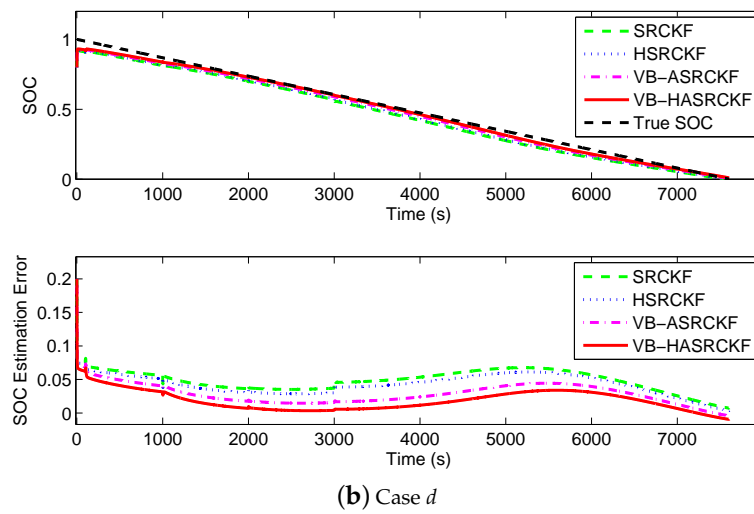


Figure 8. SOC estimation results of four filters in a constant-current discharge test under cases *c* and *d*.

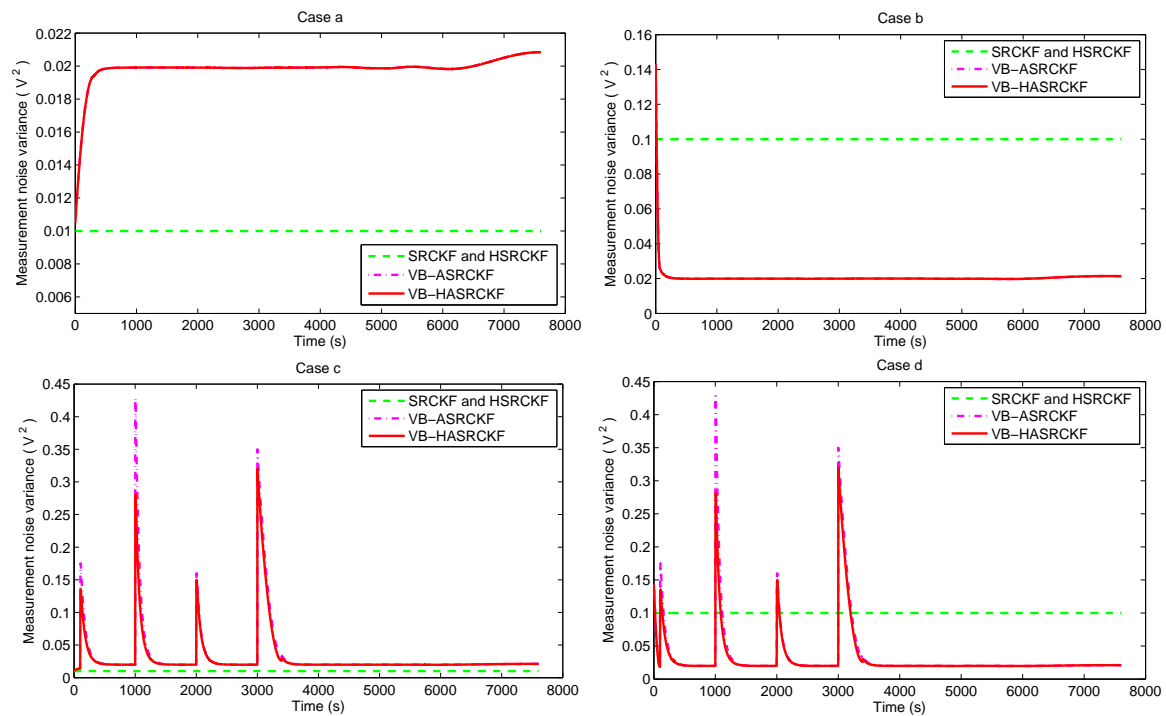


Figure 9. The measurement noise variances in a constant-current discharge test under four cases.

Table 1. The maximum and mean absolute estimation errors of four filters in a constant-current discharge test under four cases. MaE = maximum absolute error, MeE = mean absolute error.

	Case <i>a</i>		Case <i>b</i>		Case <i>c</i>		Case <i>d</i>	
	MaE	MeE	MaE	MeE	MaE	MeE	MaE	MeE
SRCKF	1.52%	0.69%	5.51%	2.24%	6.92%	3.50%	8.15%	4.84%
HSRCKF	1.84%	0.76%	5.51%	2.24%	6.68%	2.47%	7.76%	4.25%
VB-ASRCKF	2.00%	0.67%	2.02%	0.67%	7.00%	2.85%	7.30%	2.85%
VB-HASRCKF	1.97%	0.70%	2.01%	0.70%	6.62%	1.91%	6.73%	1.91%

As given above, the measurement noise variances of SRCKF and HSRCKF were mistuned in case *b*, and the initial estimates of the measurement variances of VB-ASRCKF and VB-HASRCKF are also mistuned. From the estimation results shown in Figure 7b, we can see that the SOC estimation accuracy of SRCKF and HSRCKF are dramatically declined compared with case *a*, but VB-ASRCKF and VB-HASRCKF are almost not affected by the mistuning. The estimated measurement noise variances, as shown in Figure 9, still maintain at about 0.02. This illustrates that the VB-based methods have good adaptivity to modeling error by simultaneously estimating the measurement noise variance with the SOC, while SRCKF and HSRCKF have no ability to handle this well.

In case *c*, some outliers in the voltage and current measurements appeared. The SOC estimation results are presented in Figure 8a. It is clear that VB-HASRCKF and HSRCKF outperform the other two filters in SOC estimation accuracy. It demonstrates that VB-HASRCKF and HSRCKF exhibit robustness to the outliers. In addition, VB-ASRCKF has a more accurate SOC estimation than SRCKF, probably due to the VB method being able to improve the robustness a little bit through the adaptation of the measurement noise variance. This is revealed by the estimated measurement noise variances of VB-ASRCKF and VB-HASRCKF, as given in Figure 9, which are dramatically increased when outliers emerge.

More seriously, in case *d*, there is both mistuned measurement noise variance and outliers in the measurements. The SOC estimation results are shown in Figure 8b. Clearly, VB-HASRCKF gives the best performance and SRCKF exhibits the worst performance. It can be explained by VB-HASRCKF inheriting the virtue of robustness of Huber's M-estimation and the adaptivity of the VB method. Therefore, the proposed VB-HASRCKF is the most robust and adaptive among these filters.

In addition, the computation times of the four filters under constant-current discharge test are shown in Table 2. It is clear that VB-HASRCKF has the maximum time of computation, and SRCKF has the minimum time of computation. But the difference is not obvious. That is, the proposed VB-HASRCKF shows performance improvement at the cost of a little higher computation complexity.

Table 2. Computation time of the four filters under different tests.

	Constant Current Discharge Test	UDDS Test
SRCKF	12.1816 s	30.1736 s
HSRCKF	12.4577 s	31.1709 s
VB-ASRCKF	13.1058 s	32.7837 s
VB-HASRCKF	14.1003 s	35.4377 s

5.3. SOC Estimation Experimental Results under UDDS Test

To evaluate the SOC estimation performance under dynamic loading profiles, a typical driving cycle, urban dynamometer driving schedule (UDDS), was performed on the battery cell. According to the actual tolerable currents of the lithium-ion battery cell, the loading currents were scaled down, as shown in Figure 10. The maximum current is 3.35A, and the minimum current is 0.01A. The initial SOC value was set to 0.8. The process noise covariance was set as $Q_k = 1 \times 10^{-8} I_2$. The measurement noise variances used for SRCKF and HSRCKF were both set as $R_k = 0.01$ in cases *a* and *c* but mistuned to $R_k = 0.1$ in cases *b* and *d*. The initial parameter values of VB-based filters were $v_0 = 10$, $V_0 = 0.1$ in cases *a* and *c*, while $v_0 = 10$, $V_0 = 1$ were assumed in cases *b* and *d*. As can be seen in Figure 11, the outliers in voltage measurements were added at time $k = 500$ s, 1000 s, 1500 s, 6200 s, 11,000 s, and 15,600 s, with a duration of 5–15 s in cases *c* and *d*.

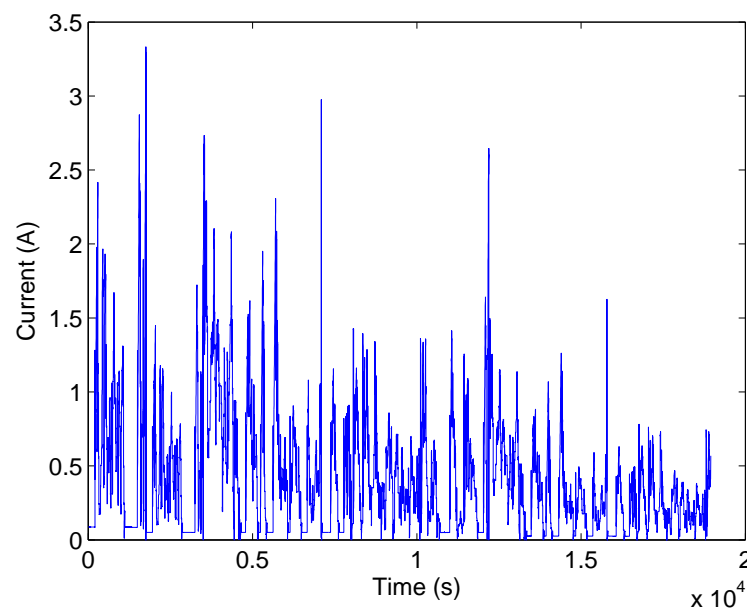


Figure 10. Current profiles in the UDDS test.

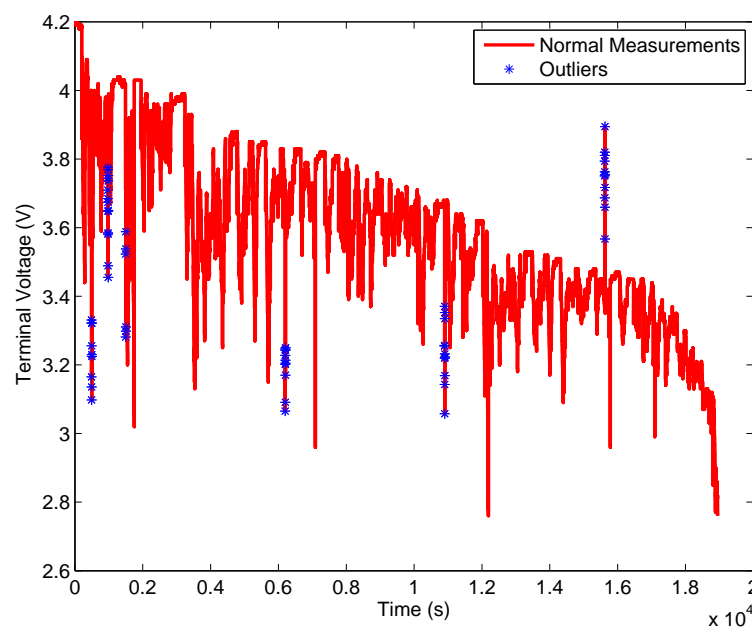


Figure 11. The outlying voltage and current measurements in the UDDS test under cases *c* and *d*.

Figures 12 and 13 present the SOC estimation results of the four filters under four cases. The maximum and mean absolute SOC estimation errors of the four filters are shown in Table 3. Figure 14 depicts the assumed and estimated measurement noise variances of the four filters. It can be seen that the estimated measurement noise variances of VB-ASRCKF and VB-HASRCKF are closer to the assumed values of SRCKF and HSRCKF in case *a*. It shows that the assumed measurement noise variance is consistent with the actual value. Thus, no significant difference occurs in SOC estimation accuracy between the four filters in case *a*. But in case *b*, VB-ASRCKF and VB-HASRCKF have more accurate SOC estimations than SRCKF and HSRCKF due to the adaptivity of the VB methods.

In case *c*, HSRCKF and VB-HASRCKF exhibit higher accuracy than the other two filters. It means that Huber's M-estimation based methods are more robust to outliers. Moreover, as given in Figure 14, the estimated measurement noise variances of VB-ASRCKF and VB-HASRCKF increase notably when

an outlier appears. It illustrates that the VB-based filter can adapt the measurement noise variance online according to the actual situation. This is why VB-ASRCKF has more accurate SOC estimation than SRCKF in the presence of outliers. In case *d*, VB-HASRCKF has the most accurate SOC estimation. The mistuned measurement noise variance and outliers in measurements have a negligible effect on VB-HASRCKF, while the effect is obvious for the other three filters.

The computation times of the four filters under the UDDS test are shown in Table 2. It can be seen that the computation time of VB-HASRCKF is 35.4377 s, while it is 30.1736 s for SRCKF. It shows that VB-HASRCKF has a little higher computation complexity.

In a word, by these comparison results, we can conclude that the proposed VB-HASRCKF algorithm has more accurate and more stable SOC estimation than the other three filters at the price of a little more computation time.

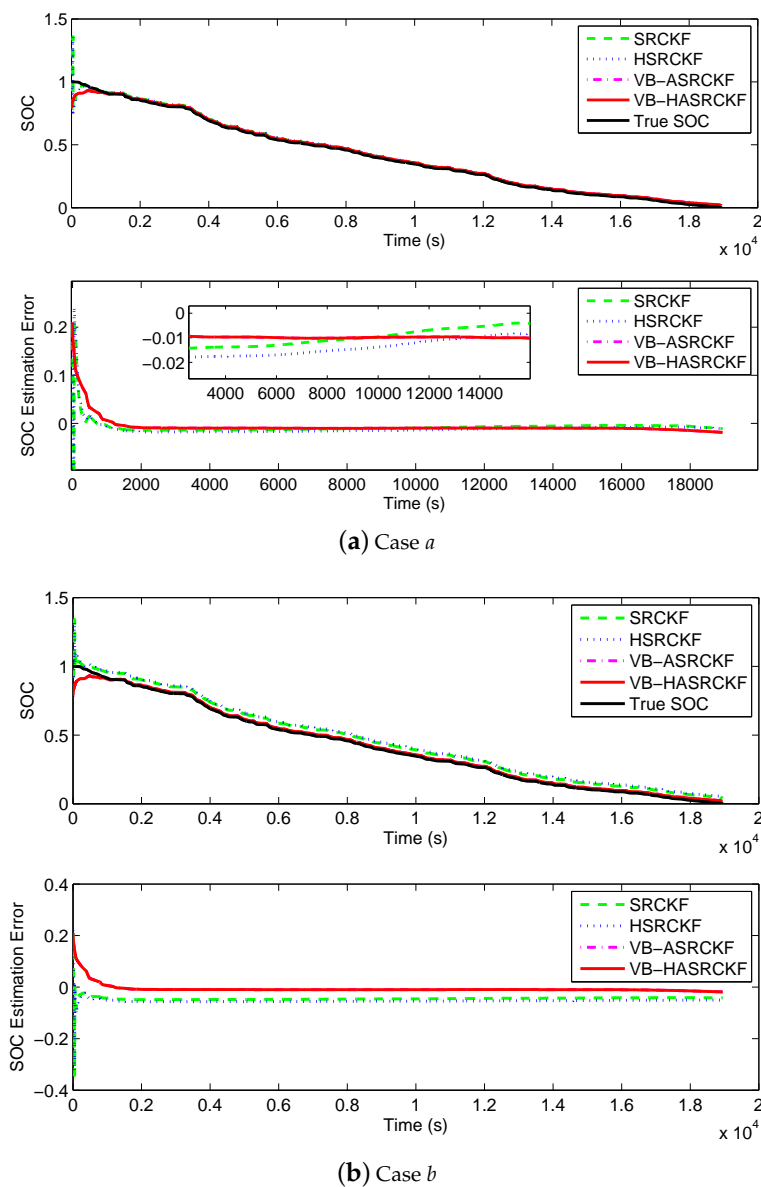


Figure 12. SOC estimation results of four filters in the UDDS test under cases *a* and *b*.

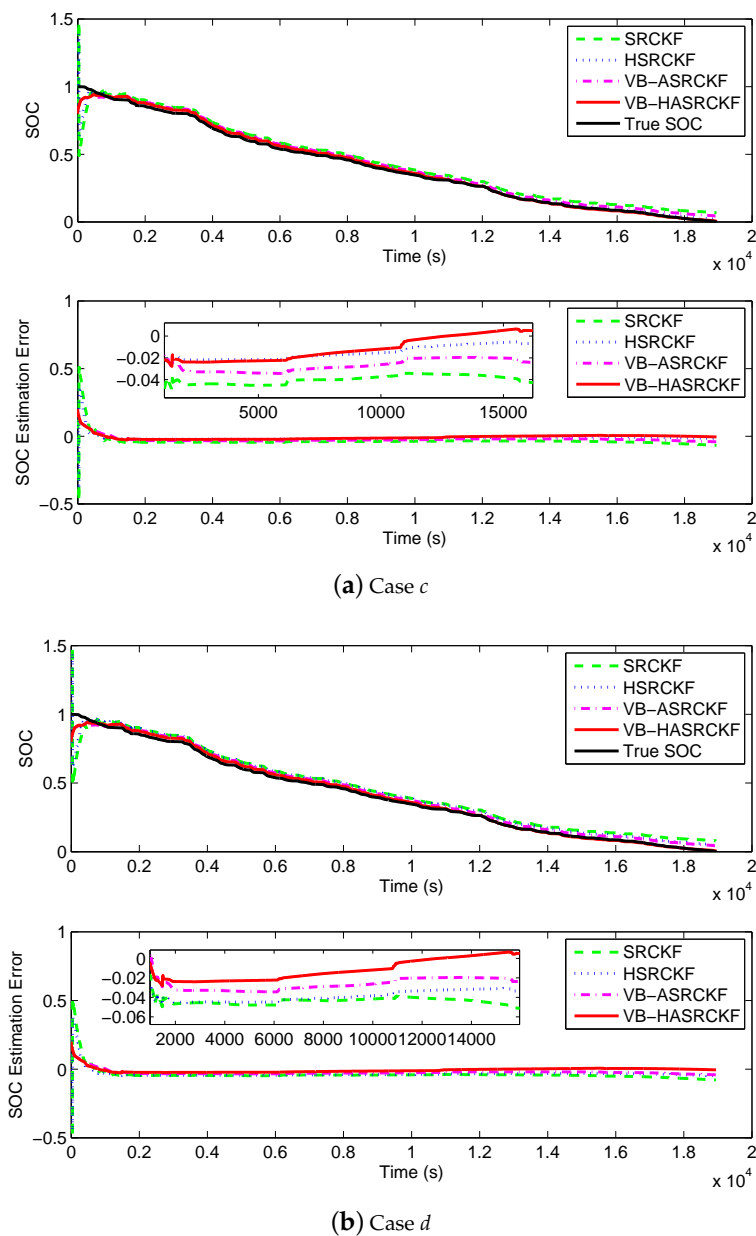


Figure 13. SOC estimation results of four filters in the UDDS test under cases *c* and *d*.

Table 3. The maximum and mean absolute estimation errors of four filters (after 10 min) in the UDDS test under four cases.

	Case <i>a</i>		Case <i>b</i>		Case <i>c</i>		Case <i>d</i>	
	MaE	MeE	MaE	MeE	MaE	MeE	MaE	MeE
SRCKF	1.46%	0.91%	4.87%	4.49%	6.72%	4.14%	7.88%	4.63%
HSRCKF	1.80%	1.28%	5.68%	5.38%	2.49%	1.44%	4.77%	3.85%
VB-ASRCKF	2.85%	1.03%	2.88%	1.03%	4.15%	2.71%	4.22%	2.71%
VB-HASRCKF	2.85%	1.03%	2.84%	1.03%	2.80%	1.18%	2.96%	1.18%

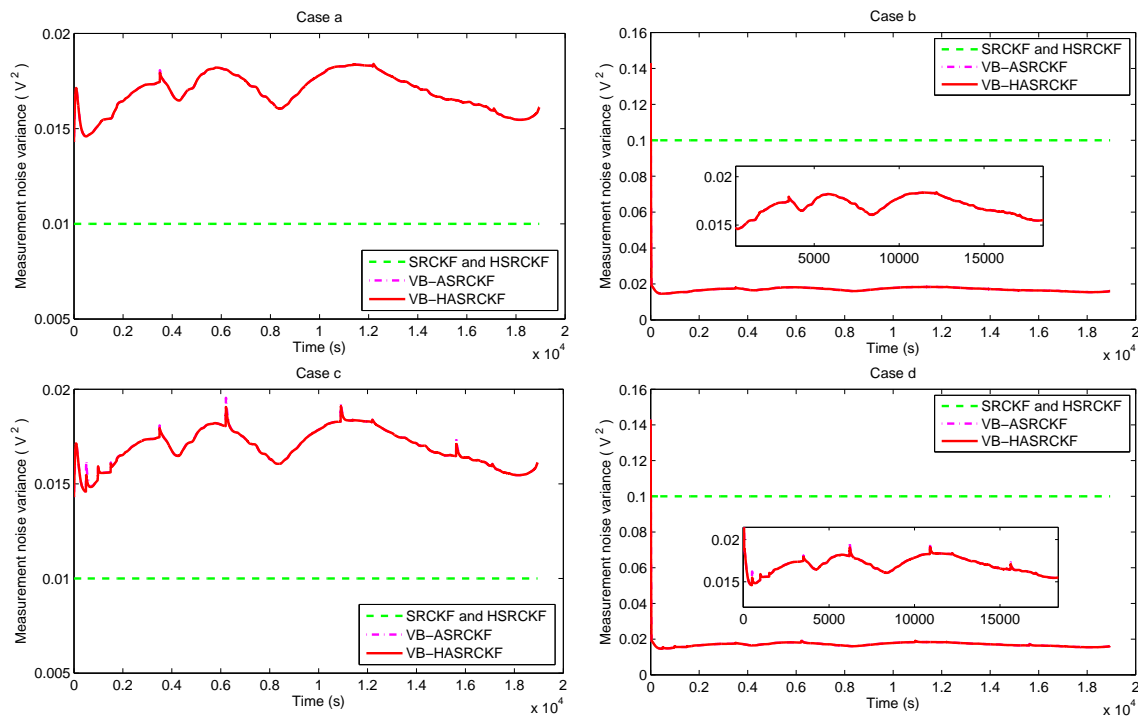


Figure 14. The measurement variances in the UDDS test under four cases.

6. Conclusions

Aiming to improve the accuracy and robustness of the SOC estimation of the lithium-ion battery under the condition of unknown or time-varying measurement noise covariance and outliers in the measurements, an adaptive and robust square root cubature Kalman filter based on variational Bayesian approximation and Huber's M-estimation (VB-HASRCKF) is proposed in this paper. The measurement noise covariance is simultaneously estimated with the SOC to account for battery model uncertainties and measurement noise covariance uncertainties, reducing the impact of model mismatch. Meanwhile, the outlying current and voltage measurements caused by adverse operating conditions are accounted for by Huber's M-estimation. Through experiments under a constant-current discharge test and a UDDS test, the effectiveness and superiority of the proposed algorithm were verified by comparison with SRCKF, HSRCKF, and VB-ASRCKF in terms of SOC estimation accuracy and robustness. Especially when there is both mistuned measurement noise covariance and outliers in the measurements, the proposed VB-HASRCKF exhibits significant performance superiority, although with a little higher computation complexity.

In addition, some comments should be made about the performance comparison with the data-driven method. As mentioned in [12], the data-driven method may be divergent with bad parameter selection when the training data cannot completely cover the present operating conditions. That is to say, if the training data does not contain the outliers in current and voltage measurements and the parameters are not appropriately chosen, the data-driven method may not exhibit as good a performance in SOC estimation accuracy as our proposed method. If the training sample set considers the case of outliers, it may have better performance than our proposed method. Even in this case, it does not mean that our method is meaningless. There is no need for a lot of training data and a large amount of computation for our method, which in itself is an advantage over the data-driven method. Of course, we will undertake a deeper comparative study on the performance of the model-based method and the data-driven method based on enough experimental data in our future work. In addition, a combination of the data-driven method and the Kalman filter-based method needs to be further studied so as to

develop their strengths and compensate their weaknesses. Uncertainties in battery capacity should also be particularly considered in future work to account for battery aging.

Author Contributions: J.H. conceived this paper, designed the experiments, and analyzed the data; H.H. did the investigation; T.G. and Y.Z. performed the experiments; Y.Y. revised the paper and provided some valuable suggestions.

Funding: This research was funded by the Fundamental Research Funds for the Central Universities (No. 3102019ZX020), Shaanxi Provincial Key Research and Development Programs (No. 2017ZDXM-GY-06, No. 2017GY-057, 2019GY-003), and Xi'an Science and Technology Planning Project–Scientific and Technological Innovation Guidance Project (No. 201805042YD20CG26 (8)).

Conflicts of Interest: The authors declare no conflict of interest.

Abbreviations

The following abbreviations are used in this manuscript:

ACKF	Adaptive Cubature Kalman Filter
ALS	Autocovariance Least Squares
ASRCKF	Adaptive Square Root Cubature Kalman Filter
ANN	Artificial Neural Network
BESS	Battery Energy Storage System
BMS	Battery Management System
CC	Coulomb Counting
CE	Coulomb Efficiency
CKF	Cubature Kalman Filter
ECM	Equivalent Circuit Model
EKF	Extended Kalman Filter
EV	Electric Vehicle
FL	Fuzzy Logic
IW	Inverse Wishart
KF	Kalman Filter
KL	Kullback–Leibler
MM	Multiple Model
OCV	Open-Circuit Voltage
PF	Particle Filter
RC	Resistor–Capacitor
SOC	State Of Charge
SVM	Support Vector Machine
SRCKF	Square Root Cubature Kalman Filter
UDDS	Urban Dynamometer Driving Schedule
UKF	Unscented Kalman Filter
VB	Variational Bayesian

References

1. Yu, Q.; Xiong, R.; Lin, C.; Shen, W.; Deng, J. Lithium-ion battery parameters and state-of-charge joint estimation based on H-infinity and unscented Kalman filters. *IEEE Trans. Veh. Technol.* **2017**, *66*, 8693–8701. [\[CrossRef\]](#)
2. Huang, C.; Wang, Z.; Zhao, Z.; Wang, L.; Lai, C.S.; Wang, D. Robustness Evaluation of Extended and Unscented Kalman Filter for Battery State of Charge Estimation. *IEEE Access* **2018**, *6*, 27617–27628. [\[CrossRef\]](#)
3. He, W.; Williard, N.; Chen, C.; Pecht, M. State of charge estimation for Li-ion batteries using neural network modeling and unscented Kalman filter-based error cancellation. *Int. J. Elect. Power Energy Syst.* **2014**, *62*, 783–791. [\[CrossRef\]](#)
4. Zhao, W.; Kong, X.; Wang, C. Combined estimation of the state of charge of a lithium battery based on a back-propagation- adaptive Kalman filter algorithm. *Proc. Inst. Mech. Eng. Part D* **2018**, *232*, 357–366. [\[CrossRef\]](#)

5. Charkhgard, M.; Farrokhi, M. State-of-charge estimation for lithium-ion batteries using neural networks and EKF. *IEEE Trans. Ind. Electron.* **2010**, *57*, 4178–4187. [\[CrossRef\]](#)
6. Singh, P.; Vinjamuri, R.; Wang, X.; Reisner, D. Design and implementation of a fuzzy logic-based state-of-charge meter for Li-ion batteries used in portable defibrillators. *J. Power Sources* **2006**, *162*, 829–836. [\[CrossRef\]](#)
7. Cai, C.H.; Du, D.; Liu, Z.Y. Battery state-of-charge (SOC) estimation using adaptive neuro-fuzzy inference system (ANFIS). In Proceedings of the 12th IEEE International Conference on Fuzzy Systems, St Louis, MO, USA, 25–28 May 2003; Volume 2, pp. 1068–1073.
8. Awadallah, M.A.; Venkatesh, B. Accuracy improvement of SOC estimation in lithium-ion batteries. *J. Energy Storage* **2016**, *6*, 95–104. [\[CrossRef\]](#)
9. Hu, J.N.; Hu, J.J.; Lin, H.B.; Li, X.P.; Jiang, C.L.; Qiu, X.H.; Li, W.S. State-of-charge estimation for battery management system using optimized support vectormachine for regression. *J. Power Sources* **2014**, *269*, 682–693. [\[CrossRef\]](#)
10. Sheng, H.; Xiao, J. Electric vehicle state of charge estimation: Nonlinear correlation and fuzzy support vector machine. *J. Power Sources* **2015**, *281*, 131–137. [\[CrossRef\]](#)
11. Wu, X.; Mi, L.; Tan, W.; Qin, J.L.; Zhao, M.N. State of charge (SOC) estimation of Ni-MH battery based on least square support vector machines. *Adv. Mater. Res.* **2011**, *211*, 1204–1209. [\[CrossRef\]](#)
12. Xiong, R.; Cao, J.; Yu, Q.; He, H.; Sun, F. Critical review on the battery state of charge estimation methods for electric vehicles. *IEEE Access* **2018**, *6*, 1832–1843. [\[CrossRef\]](#)
13. Xu, J.; Mi, C.C.; Cao, B.; Deng, J.; Chen, Z.; Li, S. The state of charge estimation of lithium-ion batteries based on a proportional-integral observer. *IEEE Trans. Veh. Technol.* **2014**, *63*, 1614–1621.
14. Huangfu, Y.; Xu, J.; Zhao, D.; Liu, Y.; Gao, F. A novel battery state of charge estimation method based on a super-twisting sliding mode observer. *Energies* **2018**, *11*, 1211. [\[CrossRef\]](#)
15. Plett, G.L. Extended Kalman filtering for battery management systems of LiPB-based HEV battery packs: Part 3. State and parameter estimation. *J. Power Sources* **2004**, *134*, 277–292. [\[CrossRef\]](#)
16. He, W.; Williard, N.; Chen, C.; Pecht, M. State of charge estimation for electric vehicle batteries using unscented kalman filtering. *Microelectron. Reliab.* **2013**, *53*, 840–847. [\[CrossRef\]](#)
17. Li, Y.; Wang, C.; Gong, J. A multi-model probability SOC fusion estimation approach using an improved adaptive unscented Kalman filter technique. *Energy* **2017**, *141*, 1402–1415. [\[CrossRef\]](#)
18. Peng, S.; Chen, C.; Shi, H.; Yao, Z. State of charge estimation of battery energy storage systems based on adaptive unscented Kalman filter with a noise statistics estimator. *IEEE Access* **2017**, *5*, 13202–1312. [\[CrossRef\]](#)
19. Wang, X.; Song, Z.; Yang, K.; Yin, X.; Geng, Y.; Wang, J. State of Charge Estimation for Lithium-Bismuth Liquid Metal Batteries. *Energies* **2019**, *12*, 183. [\[CrossRef\]](#)
20. Xia, B.; Wang, H.; Tian, Y.; Wang, M.; Sun, W.; Xu, Z. State of charge estimation of lithium-ion batteries using an adaptive cubature Kalman filter. *Energies* **2015**, *8*, 5916–5936. [\[CrossRef\]](#)
21. Zeng, Z.; Tian, J.; Li, D.; Tian, Y. An online state of charge estimation algorithm for lithium-ion batteries using an improved adaptive cubature Kalman filter. *Energies* **2018**, *11*, 59. [\[CrossRef\]](#)
22. Cui, X.; Jing, Z.; Luo, M.; Guo, Y.; Qiao, H. A New Method for State of Charge Estimation of Lithium-Ion Batteries Using Square Root Cubature Kalman Filter. *Energies* **2018**, *11*, 209. [\[CrossRef\]](#)
23. Chen, L.; Xu, L.; Wang, R. State of Charge Estimation for Lithium-Ion Battery by Using Dual Square Root Cubature Kalman Filter. *Math. Probl. Eng.* **2017**, *2017*, 5489356. [\[CrossRef\]](#)
24. Liu, S.; Cui, N.; Zhang, C. An adaptive square root unscented Kalman filter approach for state of charge estimation of lithium-ion batteries. *Energies* **2017**, *10*, 1345.
25. El Din, M.S.; Abdel-Hafez, M.F.; Hussein, A.A. Enhancement in Li-ion battery cell state-of-charge estimation under uncertain model statistics. *IEEE Trans. Veh. Technol.* **2016**, *65*, 4608–4618. [\[CrossRef\]](#)
26. Charkhgard, M.; Zarif, M.H. Design of adaptive H ∞ filter for implementing on state of- charge estimation based on battery state-of-charge-varying modelling. *IET Power Electron.* **2015**, *8*, 1825–1833. [\[CrossRef\]](#)
27. Zhao, L.; Liu, Z.; Ji, G. Lithium-ion battery state of charge estimation with model parameters adaptation using H ∞ extended Kalman filter. *Control Eng. Pract.* **2018**, *81*, 114–128. [\[CrossRef\]](#)
28. Wei, Z.; Leng, F.; He, Z.; Zhang, W.; Li, K. Online state of charge and state of health estimation for a Lithium-Ion battery based on a data-model fusion method. *Energies* **2018**, *11*, 1810. [\[CrossRef\]](#)
29. Sarkka, S.; Nummenmaa, A. Recursive noise adaptive Kalman filtering by variational Bayesian approximations. *IEEE Trans. Automat. Contr.* **2009**, *54*, 596–600. [\[CrossRef\]](#)

30. Li, K.; Chang, L.; Hu, B. A variational Bayesian-based unscented Kalman filter with both adaptivity and robustness. *IEEE Sens. J.* **2016**, *16*, 6966–6976. [[CrossRef](#)]
31. Sun, J.; Zhou, J.; Li, X. R. State estimation for systems with unknown inputs based on variational Bayes method. In Proceedings of the 15th International Conference on Information Fusion, Singapore, 9–12 July 2012; pp. 983–990.
32. Hou, J.; Yang, Y.; Gao, T. Variational Bayesian based adaptive shifted Rayleigh filter for bearings-only tracking in clutters. *Sensors* **2019**, *19*, 1512. [[CrossRef](#)]
33. Hou, J.; Yang, Y.; He, H.; Gao, T. Adaptive Dual Extended Kalman Filter Based on Variational Bayesian Approximation for Joint Estimation of Lithium-Ion Battery State of Charge and Model Parameters. *Appl. Sci.* **2019**, *9*, 1726. [[CrossRef](#)]
34. Chang, L.; Hu, B.; Chang, G.; Li, A. Huber-based novel robust unscented Kalman filter. *IET Sci. Meas. Technol.* **2012**, *6*, 502–509. [[CrossRef](#)]
35. He, W.; Pecht, M.; Flynn, D.; Dinmohammadi, F. A Physics-Based Electrochemical Model for Lithium-Ion Battery State-of-Charge Estimation Solved by an Optimised Projection-Based Method and Moving-Window Filtering. *Energies* **2018**, *11*, 2120. [[CrossRef](#)]
36. Yang, F.; Wang, D.; Zhao, Y.; Tsui, K.L.; Bae, S. J. A study of the relationship between coulombic efficiency and capacity degradation of commercial lithium-ion batteries. *Energy* **2018**, *145*, 486–495. [[CrossRef](#)]
37. Zheng, Y.; Ouyang, M.; Lu, L.; Li, J.; Zhang, Z.; Li, X. Study on the correlation between state of charge and coulombic efficiency for commercial lithium ion batteries. *J. Power Sources* **2015**, *289*, 81–90. [[CrossRef](#)]
38. Wang, J.; Cao, B.; Chen, Q.; Wang, F. Combined state of charge estimator for electric vehicle battery pack. *Control Eng. Pract.* **2007**, *15*, 1569–1576. [[CrossRef](#)]
39. Smith, A.J.; Burns, J.C.; Dahn, J.R. A high precision study of the Coulombic efficiency of Li-ion batteries. *Electrochem. Solid-State Lett.* **2010**, *13*, A177–A179. [[CrossRef](#)]
40. Wang, Q.; Kang, J.; Tan, Z.; Luo, M. An online method to simultaneously identify the parameters and estimate states for lithium ion batteries. *Electrochim. Acta* **2018**, *289*, 376–388. [[CrossRef](#)]



© 2019 by the authors. Licensee MDPI, Basel, Switzerland. This article is an open access article distributed under the terms and conditions of the Creative Commons Attribution (CC BY) license (<http://creativecommons.org/licenses/by/4.0/>).